Short Papers

Enhancing Light Blob Detection for Intelligent Headlight Control Using Lane Detection

Sungmin Eum, *Member, IEEE*, and
Ho Gi Jung, *Senior Member, IEEE*

***Abstract*—In this paper, we propose an enhanced method for detecting light blobs (LBs) for intelligent headlight control (IHC). The main function of the IHC system is to automatically convert high-beam headlights to low beam when vehicles are found in the vicinity. Thus, to implement the IHC, it is necessary to detect preceding or oncoming vehicles. Generally, this process of detecting vehicles is done by detecting LBs in the images. Previous works regarding LB detection can largely be categorized into two approaches by the image type they use: low-exposure (LE) images or autoexposure (AE) images. While they each have their own strengths and weaknesses, the proposed method combines them by integrating the use of the partial region of the AE image confined by the lane detection information and the LE image. Consequently, the proposed method detects headlights at various distances and taillights at close distances using LE images while handling taillights at distant locations by exploiting the confined AE images. This approach enhances the performance of detecting the distant LBs while maintaining low false detections.**

***Index Terms*—Intelligent headlight control (IHC), lane detection, light blob (LB) detection, low-exposure (LE) image, vanishing-point estimation.**

I. Introduction

To drive safely at night, high-beam headlights must be kept turned on unless other vehicles are found within a certain distance from the ego-vehicle [5]. However, if high beams are not converted to low beams at the appropriate moment, glare from these lights can blind oncoming or preceding drivers, which could lead to serious traffic accidents. Based on these concerns, numerous drivers are reported to be rather negligent in actively converting between high and low beams. To solve such problems, intelligent headlight control (IHC) systems, which automatically control the headlights, are being investigated by numerous researchers.

Nighttime vehicle detection (NVD) is essential in implementing an IHC system. As mentioned in [1] and [2], it is difficult to detect a vehicle at nighttime using appearance-based features since most vehicles are not visible in the dark. Thus, vehicles in nighttime are generally located by detecting the light blobs (LBs), which result from headlights or taillights. In general, a moving vehicle at night carries several light sources such as headlights or taillights, and those light sources appear on the image as LBs, which are noticeably brighter than the region around them. Therefore, most of the previous NVD methods tend to detect the LBs, which are assumed to represent the light sources. Simultaneously, those light sources are being equated with those vehicles at night from which distinctive appearance features cannot be extracted.

Locating a vehicle in nighttime by detecting LBs can be divided into two different methods. One is by using images captured under autoexposure (AE) settings [2]–[12]. In this method, bright region detection is carried out, followed by an appearance-based classification to determine the identity of the LB (e.g., headlights, taillights, or streetlight). The other approach, on the contrary, exploits low-exposure (LE) images and detects LBs with strong intensity by thresholding [13]–[15]. In this paper, these two methods are named and considered as AE-image-based and LE-image-based methods, respectively.

In most previous literature dealing with NVD, LBs are usually detected by using AE images. AE-image-based LB detection can be largely categorized into Laplacian of Gaussian (LoG) filtering [2], [9], [16]–[18] and adaptive thresholding [2], [9], [10]–[12]. Despite the fact that AE images have been used extensively, LBs generated by light sources and those from nonlight sources (e.g., reflectors) can be both observed as saturated in these images. This, in turn, makes it difficult to discriminate LBs induced by light sources from the others if they are being searched by detecting comparatively bright regions.

Meanwhile, LE-image-based methods [13]–[15] exploit the images taken under the LE setting, which suppresses most of the unwanted low-power LBs. As mentioned in [14], LBs induced by light sources are discriminated from LBs generated by nonlight sources by applying a fixed thresholding to a given LE image. Although LE-image-based methods have their advantage in efficiently withholding the *undesired* LBs, which are mostly induced by reflectors or traffic signs, they tend to suffer from having a shorter detection distance innately caused by LE. Based on such characteristics, using LE-image-based methods in detecting vehicles in the near distance (up to 100 m) for forward collision warning (FCW) systems may be suitable [14]. However, exploiting only the LE image is said to be insufficient for IHC systems since those systems should be able to detect vehicles in distant (400–600 m) locations to control the headlights at the appropriate moment.

To overcome such limitations of the LE-image-based method in being unable to detect distantly located vehicles (LBs) while maintaining its advantages, we propose a novel LB detection method that combines usage of both LE and AE images supported by lane detection results. In the proposed method, headlights in distant and near locations, along with near taillights, are detected by applying a fixed threshold value into LE images. Meanwhile, to detect taillights in distant locations that tend to have comparatively lower radiation power, a LoG-based LB detection method is applied into a specific portion of the AE image, which corresponds to distant locations of the ego-lane. LoG and lane-detection-result-driven AE images in detecting distant taillights are exploited based on the following facts: 1) Distant taillights that are in the interests of IHC systems are located on the lanes on which the ego-vehicle is driving, and 2) distant taillights are mostly exhibited as bright circular shapes of similar sizes. By constraining the region-of-interest (ROI) of AE images for the purpose of detecting distantly located LBs using the lane detection results, the drawback (short detection range) of LE-image-based LB detection can be overcome. Note that only the specific region of an AE image is used to prevent numerous false detections if the LB detection process were to be applied to the whole region of the

Manuscript received June 18, 2012; revised September 24, 2012 and November 29, 2012; accepted December 6, 2012. Date of publication January 9, 2013; date of current version May 29, 2013. The Associate Editor for this paper was P. Grisleri.

S. Eum is with the Research Institute of Automotive Electronics and Control, Hanyang University, Seoul 133-791, Korea.

H. G. Jung is with the Department of Automotive Engineering, Hanyang University, Seoul 133-791, Korea (e-mail: hogijung@hanyang.ac.kr).

Color versions of one or more of the figures in this paper are available online at http://ieeexplore.ieee.org.

Digital Object Identifier 10.1109/TITS.2012.2233736

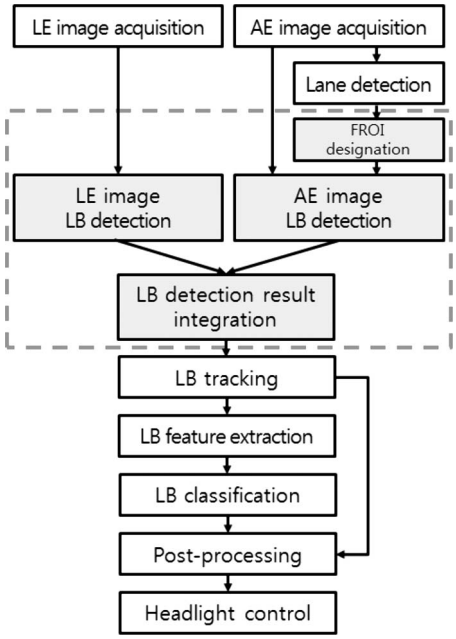

Fig. 1. System block diagram for IHC using lane detection.

given image. In addition, since IHC systems are generally required to turn off the high-beam headlights in urban areas, streetlights that cast lights upon the ego-lane are included as the detection target, along with headlights and taillights. Experimental results clearly show that the proposed LB detection method outperforms the previous methods.

II. Intelligent Headlight Control System Architecture

An IHC system architecture that includes the proposed NVD method (based on the LB detection algorithm) is depicted in Fig. 1. The dotted rectangle in the figure indicates the LB detection algorithm that we propose. Here, the whole process of the IHC system is briefly explained.

In this system, two types of images with different exposure settings (LE and AE images) are being used to detect the LBs from the vehicles. In our system, these two images, LE and AE images, are simultaneously captured (using a single camera) with a very short exposure time. Based on the fact that the exposure time of the LE image is negligibly short, it is reasonable to assume that a set of consecutively captured LE and AE images represent more or less the same scene. After being captured, each of the images is exploited in detecting two different categories of LBs: While an LE image is targeted to detect distant and near headlights along with the taillights in the near distance, an AE image is used to detect distantly located taillights that, in general, are difficult to handle using only an LE image. When using an AE image, lane detection results are incorporated to confine the ROI in which distant vehicles are likely to exist. A detailed explanation on the LB detection algorithm using LE and AE images is given in Section III.

Once the LB detection process is finished using a set of LE and AE images, the detection results are integrated before being tracked by a Kalman filtering algorithm as used in general NVD systems [2], [6], [11], [13], [14], [16]–[18]. These LBs are then classified into headlights, taillights, streetlights, and nuisance lights using a pattern-recognition-based classifier to label the valid LBs for controlling the IHC system and to eliminate the unnecessary LBs at the same time. For the classification of each LB, a feature vector is defined by incorporating several features such as position, intensity, color, and

Fig. 2. Sample images of (a) AE and (b) LE types.

velocity [5], most of which are known to be effective in discriminating the LBs.

To enhance the reliability of the LB classification results, a post-processing stage is exploited. In this process, confidence values are calculated for the classification results of every tracked LB using *a posteriori*-probability-based method [20]. This stage stabilizes and enhances the classification performance by incorporating the information extracted from antecedent images before making a final decision on the identity of each LB, instead of making independent decisions for independent images. Distance to the vehicle corresponding to an LB is generally estimated by using the distance between paired LBs and y-coordinates of the LB [18].

With the exception of the LB detection algorithm in the dotted rectangle in Fig. 1, all other stages are implemented similarly to the earlier reported research. Hence, the remainder of this paper is focused on describing the newly proposed LB detection method and its performance.

III. Light Blob Detection for Intelligent Headlight Control System

Here, we explain how to effectively combine LE-image-based and AE-image-based LB detection methods by integrating the lane detection results. By making use of the confined region (distant region with respect to the ego-vehicle) of an AE image along with an LE image, the proposed method is capable of detecting distant vehicles while maintaining the advantages of the LE-image-based LB detection method.

Before we explore the detailed explanation of the proposed method further, it is necessary to go over the characteristics of LE and AE images. Since an LE image is captured in a comparatively short exposure time, only light sources with radiation power over a certain level tend to appear bright in the image, whereas the rest of the regions are blacked out, as shown in Fig. 2(b). On the contrary, an AE image is captured under an AE setting, which, in a dark environment, is captured with a comparatively longer exposure time. For this reason, various types of unwanted LBs from nonlight sources, such as traffic signs or reflectors, are being included in the AE images and tend to show appearances similar to those of the LBs induced by a light source, as depicted in Fig. 2(a).

Based on the characteristics of LE images aforementioned, not only the headlights of the oncoming vehicle in the near distance but also those in the far distance can be detected using a simple thresholding process/ Moreover, although taillights generally show lower intensity values compared with headlights, they can also be detected by applying a threshold, given that they are located in the near distance from the ego-vehicle. Thus, for the purpose of detecting headlights in near and distant locations along with taillights closely located from the ego-vehicle, the proposed method applies a simple thresholding process, as shown in Table I. Such an approach is similar to the one used in [14].

When carrying out LE-image-based LB detection, we use a fixed threshold to detect the region brighter than $\theta_{\mathrm{LE\_LB}}$ followed by the

TABLE I
PROPOSED METHODS FOR DETECTING HEADLIGHTS AND TAILLIGHTS ACCORDING TO THEIR DISTANCE

Types	Headlights	Taillights
Near	Thresholding in LE image	Thresholding In LE image
Distant	Thresholding in LE image	LoG filtering in AE image

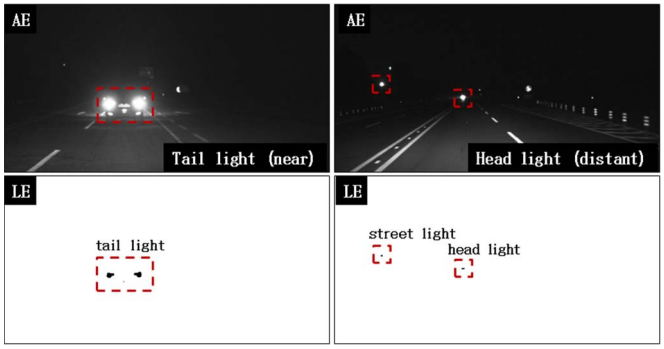

Fig. 3. LB detection using LE images.

connected component analysis to label the detected LBs. Examples of LE-image-based LB detection are shown in the bottom row of Fig. 3, which includes the detection of near taillights and distant headlights. Corresponding AE images are depicted in the top row of Fig. 3 for convenience.

Meanwhile, for the purpose of detecting distant taillights, we only exploit a specific ROI, called far ROI (hereafter FROI), where distant taillights are likely to appear. Since distant taillights appear in the image with relatively low intensity values, LE image thresholding targeted to detect near taillights and bright headlights is insufficient and is likely to fail in detecting them. If the threshold value $\theta_{\mathrm{LE\_LB}}$ for LE-image-based LB detection were to be lowered for the purpose of detecting distant taillights, unwanted false detections would occur when this same value is used to detect LBs in the near distance in LE images. In other words, lowering $\theta_{\mathrm{LE\_LB}}$ to meet the needs of detecting distant taillights would certainly take away the advantages of LE-image-based LB detection. Therefore, to detect taillights far from the ego-vehicle, it would be more reasonable to use AE images, which are capable of capturing LBs with comparatively low radiation power. In proposing our method, we took notice of the fact that distant taillights, which are in the interests of IHC systems, can only appear in a constrained region. First of all, distant taillights on the preceding vehicles can only be located on the driving lanes or adjacent lanes. Second, as a preceding vehicle drifts farther from the ego-vehicle, it approaches close to the horizon line, particularly near the vanishing point. Based on these two facts, we have defined the FROI where distant preceding vehicles can be located around the vanishing point, which is estimated by acquiring the intersection point of the left- and right-lane markings of the driving lane.

The FROI, which is in the form of a rectangle, is defined to meet the IHC system requirements. First, the lower boundary of the FROI, i.e., y_{FROI}, is defined by the maximum LB detection range of the FCW. (We are assuming that the system requirements are given.) y_{FROI} can easily be calculated using the camera geometry based on perspective range estimation model [21] given by

$$y_{\mathrm{FROI}} = k\left(\frac{f \cdot H}{Z_{\mathrm{FCW}}}\right) \tag{1}$$

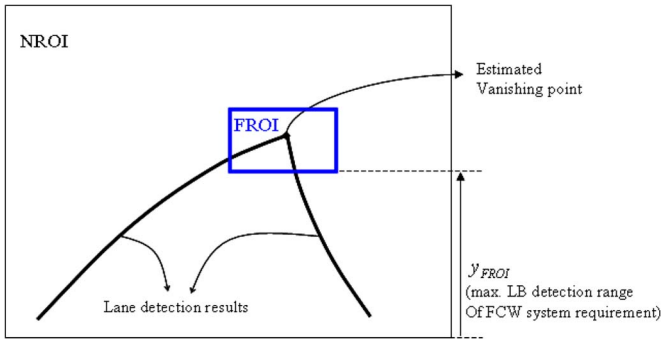

Fig. 4. Setting the FROI and NROI using lane detection.

Fig. 5. Various shapes found in taillights.

where f, H, and Z_{FCW} are the focal length, the camera height from the ground level, and the detection range of the FCW system, respectively. While the measures are in meters, k indicates the proportional factor for unit conversion from meter to pixel. Then, the width of the FROI is determined by acquiring the points on the lanes having y_{FROI} as y-coordinates, whereas the height is set by considering the average height of the common vehicles. Once the boundaries of the FROI are established during the calibration phase, they are transformed into the displacements with respect to the vanishing point. Therefore, if the vanishing point changes because of the road shape, the FROI will follow the vanishing point to be located around it. As the FROI is established based on the detected vanishing point, changes in tilt angle (or, pitching) and road curvature could be compensated to some degree. The lane detection algorithm is implemented based on the steerable filter [22], [23], which can efficiently utilize the lane information on the previous time step. The detected lane markings are fitted to a quadratic curve. For more details, see [29]. For the convenience of description, the whole image, including the FROI, is hereafter referred to as NROI (Near ROI), as shown in Fig. 4.

We now switch to the description of detecting distant taillights. Distant taillights are detected by applying LoG filtering inside the FROI, followed by a fixed-value thresholding. Although comparatively darker than the lights in the near distance, distant taillights appear in the image as blobs brighter than the regions that do not have any light sources. Moreover, despite the fact that the shape of the taillights cannot be simply defined when located in the near distance, as shown in Fig. 5, they can be characterized as similarly sized circular LBs if they are captured in distant locations far from the ego-vehicles, as shown in Fig. 6. On that account, we can conclude that distant taillights can be detected by searching for similarly sized circular blobs, or modes, which are comparatively brighter than the peripheral regions.

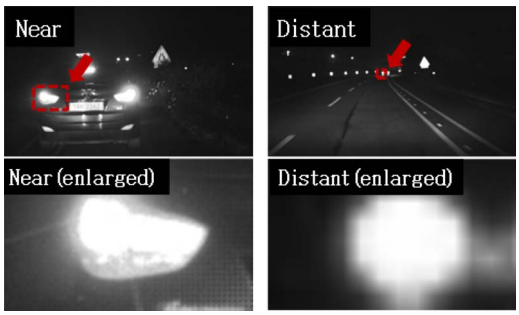

Fig. 6. Taillights of the same vehicle converging to a circular shape in distant locations.

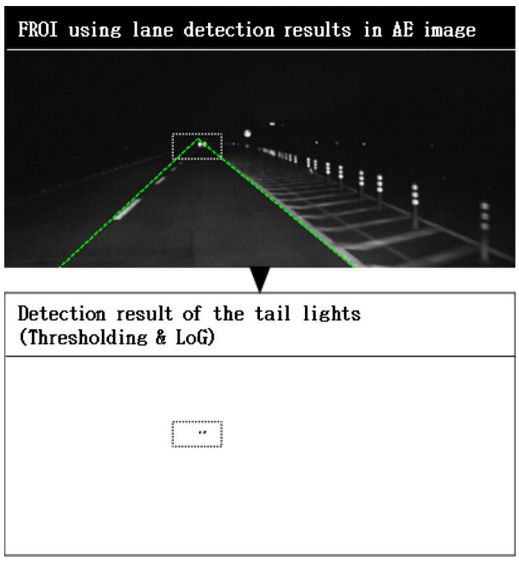

Fig. 7. Process of detecting taillights in a distant location.

To detect distant taillights having such characteristics, we have implemented the following procedure. First of all, fixed thresholding using $\theta_{\mathrm{LE\_CAND}}$ is applied to the FROI of the LE image to detect the area that is comparatively brighter than the peripheral regions. (Note that $\theta_{\mathrm{LE\_CAND}}$ is considerably smaller than $\theta_{\mathrm{LE\_LB}}$ since distant taillights are relatively dim.) Then, in this restricted area, LoG filtering is exploited for the purpose of detecting similarly sized blobs, followed by fixed thresholding with θ_{LOG} to obtain the final LB regions. It is noteworthy to mention that all taillights inside the FROI appear in almost equivalent sizes. Thus, the size parameter of the LOG filter σ_{LOG} was set as a fixed constant [25]. Fig. 7 depicts how distant taillights are detected by using the proposed method.

After both detection methods in a set of LE and AE images are carried out, detected regions are combined to finalize the detection result. If an LB is detected in the LE and AE images at the same location, the LB detected in the AE image is eliminated due to the fact that the LB detected in the LE image is more reliable than the one detected in the AE image.

IV. Parameter Settings

As aforementioned, three different parameters, i.e., $\theta_{\mathrm{LE\_LB}}$, $\theta_{\mathrm{LE\_CAND}}$, and θ_{LOG}, should be properly determined beforehand to perform the proposed LB detection inside the NROI and FROI. Here, we describe how these parameters are related and propose a practical guideline in configuring them when implementing an IHC system.

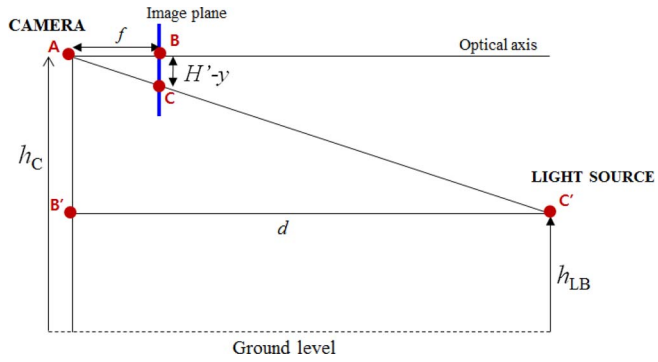

Fig. 8. Camera model.

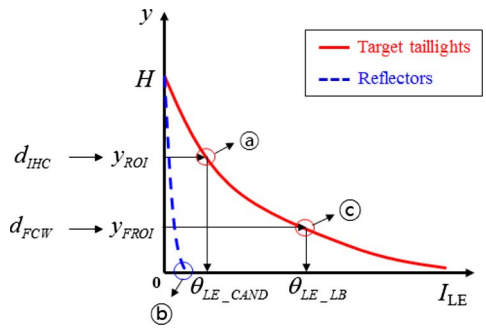

Fig. 9. Quadratic curves showing the relationship between y and I_{LE}.

To obtain the dependence between the parameters, we have constructed a model that shows the physical relationship between the camera and an LB. The model is depicted in Fig. 8. In this figure, f, H', y, and d correspond to the focal length of the camera, half of the image height, the y-coordinate of the detected LB (the bottommost coordinate is assumed to be 0), and the distance (in the direction of the optical axis) between the camera and the LB, respectively. Moreover, h_c and h_{LB} each represent the height of the camera and the LB from the ground level. Since the two triangles $\triangle ABC$ and $\triangle AB'C'$ are similar, (2), shown below, can be used to obtain (3), shown below [2], [11]. Moreover, based on the fact that the intensity of the LB on the image, i.e., I_{LE}, is inversely proportional to the square of the distance d from the camera [18], [31], and proportional to the camera exposure time τ_{LE} [30], (4), shown below, can be formularized by including a proportional constant k. By substituting (3) into (4), the relationship between the intensity of the LB and its y-coordinate can be retrieved, as in (5), shown below:

$$f : H' - y = d : h_c - h_{\mathrm{LB}} \tag{2}$$

$$d = \frac{f(h_C - h_{\mathrm{LB}})}{H' - y} \tag{3}$$

$$I_{\mathrm{LE}} = k\frac{\tau_{\mathrm{LE}}}{d^2} \tag{4}$$

$$I_{\mathrm{LE}} = k\frac{\tau_{\mathrm{LE}}(H' - y)^2}{f^2(h_C - h_{\mathrm{LB}})^2} = K\tau_{\mathrm{LE}}(H' - y)^2. \tag{5}$$

The relationship between the intensity of the LB and its y-coordinate, which is derived as in (5), can also be depicted as a graph, as shown in Fig. 9. It can be seen in the figure that the scale of the quadratic function is dependent upon the exposure time τ_{LE} of the given camera. Note that a group of LBs with similar characteristics can be represented as a single second-order curve in this figure. LBs that are not induced by the light sources, e.g., reflectors, can be depicted as the blue dotted curve since they tend to bear low radiation

power. Meanwhile, taillights, which are comparatively brighter than the reflectors, can be represented by the red curve in the figure. It is significant to note that the objective of the proposed system is to be able to correctly detect taillights (red curve) while eliminating as many nuisance lights that are not from light sources (blue dotted curve) as possible.

Let us assume that d_{FCW} is the maximum detection distance that the FCW system should satisfy, and d_{IHC} is the maximum taillight detection distance for the IHC system. y_{ROI} and y_{FROI} can be determined by measuring the y-coordinates of LBs when the preceding vehicle is located at d_{IHC} and d_{FCW}, respectively. Then, referring to the graph shown in Fig. 9, d_{FCW} and d_{IHC} can be corresponded to $\theta_{\mathrm{LE\_LB}}$ and $\theta_{\mathrm{LE\_CAND}}$, respectively. Accordingly, it can be seen that if either y-coordinate of the LB or the intensity value (or thresholding value) is determined, the other undecided value should automatically be determined by the given function. That is, $\theta_{\mathrm{LE\_LB}}$ and $\theta_{\mathrm{LE\_CAND}}$ can be determined by measuring the intensity values of LBs when the preceding vehicle is located at d_{FCW} and d_{IHC}, respectively. Since d_{FCW} and d_{IHC} is determined in advance by the requirement of the given system in general, camera exposure time τ_{LE}, which controls the scale of the curve, would be the only parameter left for the user to adjust. The following discusses how to set τ_{LE}, considering not only an ideal case but also a practical case.

The two curves in Fig. 9 depict an ideal condition where taillights and reflectors can be discriminated with a simple fixed-value thresholding process. In the figure, ⓐ, ⓑ, ⓒ each indicate the intensity of the taillight at the farthest location that an IHC system should handle, the intensity of a reflector closest from the ego-vehicle (indicating the brightest reflector), and the intensity of the taillight at the farthest location that a FCW system should handle, respectively.

The objective is to maximize the discrimination between the taillights and the reflectors by placing ⓐ on the right side of ⓑ and setting the threshold $\theta_{\mathrm{LE\_CAND}}$ between those two intensity values. If the exposure time τ_{LE} of the camera were to be increased from a small value to a larger one, the red curve (target taillights) that manifests strong radiation should recede from the y-axis comparatively faster than the blue dotted curve (reflectors). This is because reflectors, which are not induced by the light sources, are generally low in radiation. Based on this phenomena, it is reasonable to conclude that LB detection performance discriminating between the taillights and reflectors could be maximized by setting the appropriate exposure time τ_{LE}, which could place ⓐ sufficiently far from ⓑ.

However, in a more realistic situation, reflectors with considerably high reflection strength (which in turn appear with high intensity values) may exist unlike the idealistic situation shown in Fig. 9. Thus, discriminating the target taillights from the reflectors using fixed-value thresholding may not be as simply as aforementioned. LBs that correspond to the dotted areas in Fig. 10 represent such difficult situations. Since these cases cannot be fully handled by applying a fixed threshold, LB classification should also be used in conjunction with LB features such as position, velocity, or color.

Based on the previous discussions here, we propose a practical guideline in setting the parameters to be used in the proposed LB detection process for the IHC system.

1) Maximum exposure time τ_{LE} for the LE image should be chosen, which could keep most of the nonlight source pixels blacked out in the image. For instance, while the intensity variance of the ground surface in front of the ego-lane could be maintained between 3 and 4, maximum exposure time should be sufficiently reasonable.
2) Once the exposure time τ_{LE} is determined, the function between the intensity of the LB and its y-coordinate is fixed. Since d_{FCW} and d_{IHC} should be given by the system requirements, y_{ROI} and y_{FROI} can be determined by measuring the y-coordinates of LBs when the preceding vehicle is located at d_{IHC} and d_{FCW}, respectively. Similarly, $\theta_{\mathrm{LE\_LB}}$ and $\theta_{\mathrm{LE\_CAND}}$ can be determined by measuring the intensity values of LBs when the preceding vehicle is located at d_{FCW} and d_{IHC}, respectively.
3) The size parameter of the LoG filter, i.e., σ_{LOG}, should be determined, considering the average radius of the taillights detected inside the FROI of the AE images.

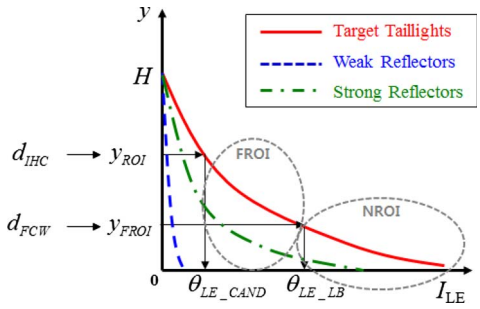

Fig. 10. Confusion caused by abnormally strong reflectors.

When implementing the proposed LB detection for the IHC system, we have referred to the previous literature [18], [19] where the practical operating range of the IHC systems is discussed. Accordingly, the maximum preceding vehicle detection range for the IHC system d_{IHC} and maximum detection (both preceding and oncoming) range for the FCW system d_{FCW} are set as 400 and 100 m, respectively. Meanwhile, the maximum oncoming vehicle detection range for the IHC system is generally set as 600 m. We have experimentally found that, if the appropriate parameters are chosen to discriminate the taillights from the reflectors, headlights on the oncoming vehicles would generally be saturated in white, thus naturally discriminating them from the nonlight source LBs.

The intensity thresholds $\theta_{\mathrm{LE\_LB}}$ and $\theta_{\mathrm{LE\_CAND}}$ are irrespective of pitching because the intensity of an LB depends only on the distance to the corresponding light source. In other words, even when the camera tilt angle changes because of pitching, the Euclidean distance to the light source does not change, and the LB intensity will not change. Therefore, even when pitching occurs, LBs can be detected using the same thresholds. Notice that the application of $\theta_{\mathrm{LE\_CAND}}$ is spatially confined by the FROI: The influence of pitching on $\theta_{\mathrm{LE\_CAND}}$ is compensated by establishing the FROI using the detected vanishing point, as explained earlier.

V. Experimental Results

The experimental sequences were acquired using a Complementary Metal-Oxide Semiconductor camera attached to the right side of the room mirror inside the windshield (1.27 m above ground level). A sensor manufactured by Aptina [27] was used for the camera. The images were captured at a speed of 30 frames/s with a resolution of 752 (width) × 480 (height) pixels.

To evaluate the detection performance of the proposed LB detection method, 24 sequences were acquired, which were composed of 37 360 frames (LE 18 680 frames, AE 18680 frames) in total. All sequences were captured at night on suburb motorways, where IHC function is expected to be mostly used [2]. These sequences were categorized into three difference scenarios: seven sequences with oncoming vehicles (headlights), 12 sequences with preceding vehicles (taillights), and five sequences that include mostly streetlights. Sample images of these three scenarios are included in Fig. 11. Fig. 11(a)–(c) depicts a set of sequential images of the preceding vehicle, oncoming vehicle, and urban area with streetlights, respectively.

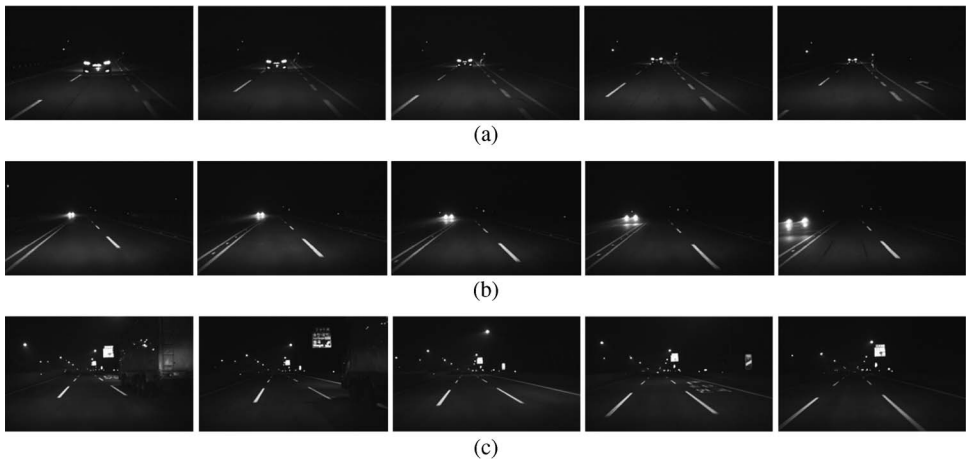

Fig. 11. Sample images from the database. (a) Preceding vehicle (taillights). (b) Oncoming vehicle (headlights). (c) Urban area (streetlights).

IHC systems should be able to correctly discriminate or perceive headlights, taillights, and streetlights to properly control the high or low beam of the ego-vehicle. Thus, to correctly evaluate the LB detection performance for practical IHC systems, we have chosen headlights, taillights, and streetlights as the target LBs of the detection process. Note that streetlights are included as detection targets because high beams should be turned off in urban areas [2], [5], [28] by conventional IHC systems. Only the LBs, whose types could be discriminated manually, were used in the detection performance evaluation by assigning the corresponding ground truths.

To show the superiority of the proposed LB detection method, we have chosen three of the most frequently used LB detection methods suggested by the previous literature, along with a method combining the two approaches similar to the proposed method: 1) applying fixed thresholding into LE images [15], [26] (method 1); 2) applying adaptive thresholding into AE images [2], [9], [10]–[12] (method 2); 3) applying LoG filtering into AE images [2], [9], [16]–[18] (method 3); and 4) combining the detection results of LE (fixed thresholding) and AE images (adaptive thresholding inside FROI).

The adaptive thresholding, which is one of the methods compared with the proposed algorithm, is implemented as follows [2]. First, fixed thresholding is applied to each input image using a very low value such as 50 (in a gray-level range having 0 to 255) to extract all potential LBs. Then, the mean and the standard deviation of the input image is calculated with the mean μ_i and the standard deviation σ_i of these extracted blobs as in (6) and (7). In the equations, N indicates the total number of extracted objects from an image. After obtaining the adaptive threshold value by using (8), LBs are extracted by thresholding from the original input image. These are shown in the following:

$$\mu = \frac{1}{N} \cdot \sum_{i=1}^{N} \mu_i \tag{6}$$

$$\sigma = \frac{1}{N} \cdot \sum_{i=1}^{N} \sigma_i \tag{7}$$

$$\text{Adaptive threshold} = \mu - K \cdot \sigma. \tag{8}$$

Among the four LB detection methods implemented for the purpose of comparing them with the proposed algorithm, method 3, which uses LoG filtering in AE images, was excluded from the performance evaluation. To detect the LBs at various distances (from the ego-vehicle) using LoG filtering, the size of the LoG filter mask should be exploited adaptively. In other words, such implementation requires the size of the LoG filter mask to be set differently for each row. This method clearly lacks practicality in the following perspectives. First, if the method is implemented by preparing a large number of LoG filter masks to be applied to different distances (different rows in the image), memory insufficiency would occur when using the algorithm in an embedded system. Second, if the method is implemented to instantly generate the LoG filter masks every time a detection process is performed, it would be difficult to carry out the LB detection in real time. Third, since the same row can be regarded as locations with similar distances from the ego-vehicle, fast Fourier transform (FFT) could be used for every row of the image to enhance the speed. However, this still lacks real-time performance since FFT should be performed repeatedly proportional to the height of the image. Finally, it is needless to say that, in applying the filters, using convolution instead of FFT would bring an even higher load to the system.

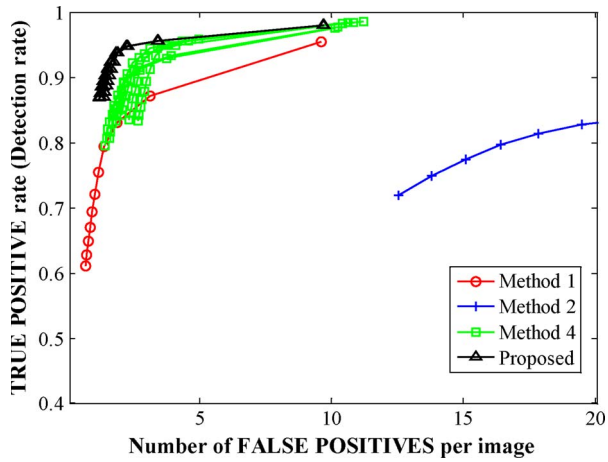

Fig. 12. Comparison of the LB detection performances (ROC curves).

The receiver operating characteristic (ROC) curves of the proposed method along with the previous approaches are depicted in Fig. 12. While the x-axis indicates the number of false positives per image, the y-axis indicates the true positive rate (detection rate) of the LB detection. We have regarded the detection result as *correctly detected*, when the center coordinate of the detected LB resides inside the ground-truth region of the corresponding LB. The detection rate is calculated by the ratio between the number of correctly detected LBs and the total number of LBs. Note that a ground-truth region of an LB

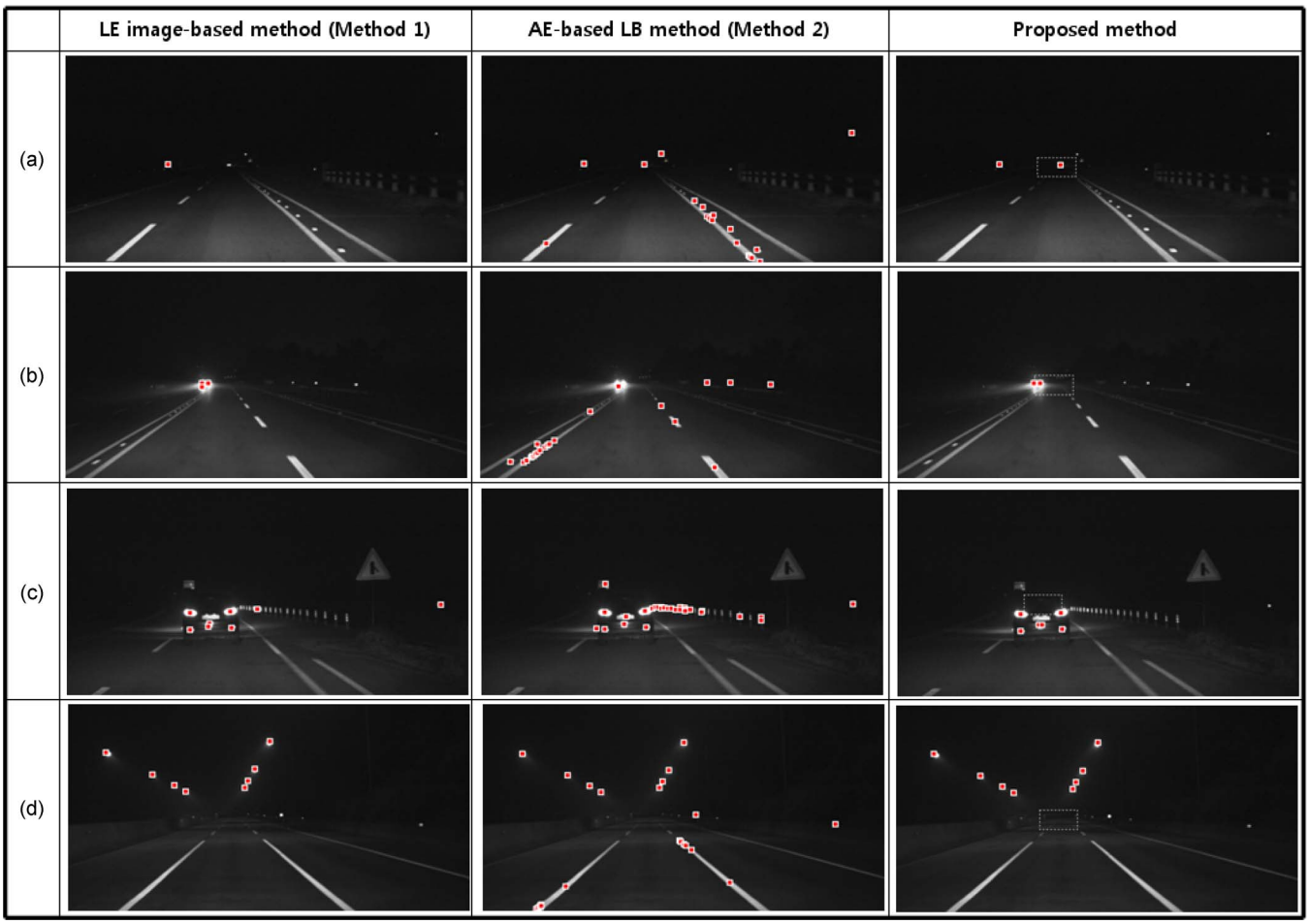

Fig. 13. Comparison of the LB detection results. The proposed method outperforms the other two previous methods.

was manually set by designating the minimum rectangle region, which accommodates the whole area of the given LB.

The ROC curve for method 1 was obtained by gradually incrementing the parameter $\theta_{\mathrm{LE\_LB}}$ used in the LE image thresholding, whereas that of method 2 was acquired by adjusting the K value used in (8). To draw the six best ROC curves for method 4, different combinations of K values (for adaptive thresholding) and LE image thresholding parameters $\theta_{\mathrm{LE\_LB}}$ were used. Finally, to acquire the six best ROC curves of the proposed method, different combinations of the thresholding parameters θ_{LOG} used in the AE-image-based detection process and LE image thresholding parameters $\theta_{\mathrm{LE\_LB}}$ were applied.

As shown in Fig. 12, to maintain low false positives by only using LE images (method 1), the detection rate drops to almost 80% due to the failure of detecting distant headlights or taillights. On the other hand, it can be analyzed that, if it is required to manage a reasonable detection rate only by using AE images (Method 2), we have to risk a large number of false positives. Meanwhile, it can be clearly seen that both method 4 and the proposed method notably outperform the other two methods. This reason lies in the fact that these two methods only utilize the constrained region of the AE images, which assists in reducing the false positives to a great extent. In particular, by observing that the proposed method achieves better performance than method 4, it can be concluded that LoG filtering is more effective than adaptive thresholding for the purpose of detecting distant taillights in AE images.

It is shown in Fig. 12 that the detection rates of the proposed method do not perfectly converge to 100%, even if the threshold parameters are sufficiently lowered. The imperfection on the detection performance can be explained by two primary reasons. First, since the proposed LB detection algorithm is mainly based on thresholding the intensity values, it sometimes fails to discriminate the closely located independent LBs and misconceives them as a single LB. Second, when the oncoming or preceding vehicles are present in considerably distant locations from the ego-vehicle, the headlights or taillights tend to appear on the image as tiny blurred blobs with a size of 2 or 3 pixels. This, in turn, makes it difficult to discriminate those LBs from the background regions having similar intensity values. Note, however, that those missing LBs were mostly found outside the range of interests (within 600 m from the ego-vehicle), which does not negatively affect the operation of conventional IHC systems.

Fig. 13 shows the LB detection results using the previous methods compared with those using the proposed method. In this figure, the center locations of the detected LBs are plotted as red dots. The first and second columns depict the detection results of LE-image-based (Method 1), and AE-image-based (Method 2) methods, respectively. While the LE-image-based method produces less false positives, it is often incapable of detecting the distant LBs. On the other hand, distant LBs can be detected using the AE-image-based method but along with numerous unwanted false positives. Meanwhile, the third column clearly shows that the proposed method, which exploits the FROI and both types of images (LE and AE), succeeds in being able to detect the distant LBs while maintaining low false positives. In particular, Fig. 13(b) and (c) shows that the proposed method generates less false positives than method 1. This is because method 1 should excessively lower the threshold $\theta_{\mathrm{LE\_LB}}$ to detect distant preceding vehicles.

Fig. 14. FROI on a curved road.

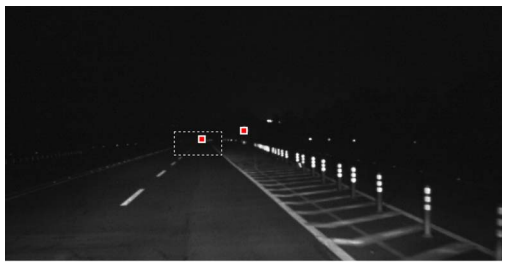

(a)

(b)

Fig. 15. Typical examples of false detection. (a) Examples of false positive. (b) Example of false negative.

Fig. 14 shows an example of FROI on a curved road. As our lane detection detects the lane markings only in relatively near distance, the distant area of the driving lane is located out of the FROI. However, if the distant area of the driving lane departs significantly from the front of the ego-vehicle, it has little meaning to an IHC system, which is developed for the removal of glare, because the light distribution of a general headlight has a very sharp shape [18]. In other words, a driver in such a distant area on a curved road will not be affected by the bright headlights emitted from the ego-vehicle.

Fig. 15(a) shows two examples of typical false positive: One on the left is caused by a taillight that is out of the detection range, and the other is caused by a traffic sign that is reflected too brightly, as shown in Fig. 10. Such a brightly reflected traffic sign is the major reason why the LB classification follows the LB detection, as shown in Fig. 1. Fig. 15(b) shows an example of typical false negative. Although there are two taillights within the detection range, only one is detected.

VI. Conclusion

This paper proposes a novel LB detection method for an IHC that effectively exploits LE images along with a portion of AE images constrained by the lane detection results. In the proposed algorithm, headlights or taillights in the near distance having high intensity values are detected applying a fixed thresholding into the LE image. Meanwhile, to detect taillights in distant locations that tend to have comparatively lower intensity values, a LoG-based LB detection method is applied into a specific portion (FROI) of the AE images, which corresponds to distant locations of the driving lane. Experimental results clearly show that the proposed method outperforms the previous approaches by enhancing the detection rates while maintaining the low false positives. Additionally, the proposed method was proven to have the ability to correctly detect streetlights in urban areas, which are also in the interest of practical IHC systems. The improvement of lane detection in nighttime is expected to improve the proposed method. In addition, adaptation of the FROI establishment according to the shape of the driving lane, such as the vertical and horizontal curvatures, is scheduled as a further study.

References

[1] Y.-L. Chen, B.-F. Wu, H.-Y. Huang, and C.-J. Fan, "A real-time vision system for nighttime vehicle detection and traffic surveillance," *IEEE Trans. Ind. Electron.*, vol. 58, no. 5, pp. 2030–2044, May 2011.

[2] P. F. Alcantarilla, L. M. Bergasa, P. Jiménez, I. Parra, D. F. Llorca, M. Sotelo, and S. Mayoral, "Automatic light beam controller for driver assistance," *Mach. Vis. Appl.*, vol. 22, no. 5, pp. 819–835, Sep. 2011.

[3] Y.-C. Lin, C.-C. Lin, L.-T. Chen, and C.-K. Chen, "Adaptive IPM-based lane filtering for night forward vehicle detection," in *Proc. 6th IEEE Conf. Ind. Electron. Appl.*, 2011, pp. 1568–1573.

[4] J. H. Connell, B. W. Herta, S. Pankanti, H. Hess, and S. Pliefke, "A fast and robust intelligent headlight controller for vehicles," in *Proc. Intell. Veh. Symp.*, 2011, pp. 703–708.

[5] Y. Li and S. Pankanti, "A performance study of an intelligent headlight control system," in *Proc. IEEE Workshop Appl. Comput. Vis.*, 2011, pp. 440–447.

[6] H.-Y. Cheng and S.-H. Hsu, "Intelligent highway traffic surveillance with self-diagnosis abilities," *IEEE Trans. Intell. Transp. Syst.*, vol. 12, no. 4, pp. 1462–1472, Dec. 2011.

[7] J. C. Rubio, J. Serrat, A. M. López, and D. Ponsa, "Multiple-target tracking for intelligent headlights control," *IEEE Trans. Intell. Transp. Syst.*, vol. 13, no. 2, pp. 594–605, Jun. 2012.

[8] W. Zhang, Q. M. J. Wu, G. Wang, and X. You, "Tracking and pairing vehicle headlight in night scenes," *IEEE Trans. Intell. Transp. Syst.*, vol. 13, no. 1, pp. 140–153, Mar. 2012.

[9] A. Jazayeri, H. Cai, J. Y. Zheng, and M. Tuceryan, "Vehicle detection and tracking in car video based on motion model," *IEEE Trans. Intell. Transp. Syst.*, vol. 12, no. 2, pp. 583–595, Jun. 2011.

[10] S. Gormer, D. Muller, S. Hold, M. Meuter, and A. Kummert, "Vehicle recognition and TTC estimation at night based on spotlight pairing," in *Proc. IEEE Int. Conf. Intell. Transp. Syst.*, 2009, pp. 1–6.

[11] P. F. Alcantarilla, L. M. Bergasa, P. Jiménez, M. A. Sotelo, I. Parra, D. Fernandez, and S. S. Mayoral, "Night time vehicle detection for driving assistance light beam controller," in *Proc. IEEE Intell. Veh. Symp.*, 2008, pp. 291–296.

[12] R. DeFauw, S. Lakshmanan, and K. V. Prasad, "A system for small target detection, tracking, and classification," in *Proc. IEEE/IEEJ/JSAI Int. Conf. Intell. Transp. Syst.*, 1999, pp. 639–644.

[13] R. O'Malley, M. Glavin, and E. Jones, "Vision-based detection and tracking of vehicles to the rear with perspective correction in low-light conditions," *IET Intell. Transp. Syst.*, vol. 5, no. 1, pp. 1–10, Mar. 2011.

[14] R. O'Malley, E. Jones, and M. Glavin, "Rear-lamp vehicle detection and tracking in low-exposure color video for night conditions," *IEEE Trans. Intell. Transp. Syst.*, vol. 11, no. 2, pp. 453–462, Jun. 2010.

[15] A. Fossati, P. Schönmann, and P. Fua, "Real-time vehicle tracking for driving assistance," *Mach. Vis. Appl.*, vol. 22, no. 2, pp. 439–448, Mar. 2011.

[16] D.-Y. Chen, J.-J. Wang, C.-H. Chen, and Y.-S. Chen, "Video-based intelligent vehicle contextual information extraction for night conditions," in *Proc. Int. Conf. Mach. Learn. Cybern.*, 2011, vol. 4, pp. 1550–1554.

[17] T. Shamm, C. V. Carlowitz, and J. M. Zöllner, "On-road vehicle detection during dusk and at night," in *Proc. IEEE Intell. Veh. Symp.*, 2010, pp. 418–423.

[18] J. Rebut, B. Bradai, J. Moizard, and A. Charpentier, "A monocular vision based advanced lighting automation system for driving assistance," in *Proc. IEEE Int. Symp. Ind. Electron.*, 2009, pp. 311–316.

[19] R. E. Kalman, "A new approach to linear filtering and prediction problems," *Trans. ASME, J. Basic Eng.*, no. 82, pp. 35–45, 1960.

[20] H. G. Jung and J. Kim, "Constructing a pedestrian recognition system with a public open database, without the necessity of re-training: An experimental study," *Pattern Anal. Appl.*, vol. 13, no. 2, pp. 223–233, May 2010.

[21] G. P. Stein, O. Mano, and A. Shashua, "Vision-based ACC with a single camera: Bounds on range and range rate accuracy," in *Proc. IEEE Intell. Veh. Symp.*, 2003, pp. 120–125.

[22] J. C. McCall and M. M. Trivedi, "Video-based lane estimation and tracking for driver assistance: Survey, system, and evaluation," *IEEE Trans. Intell. Transp. Syst.*, vol. 7, no. 1, pp. 20–37, Mar. 2006.
[23] L. Guo, K. Li, J. Wang, and X. Lian, "A robust lane detection method using steerable filters," in *Proc. 8th Int. Symp. Adv. Veh. Control*, 2006.
[24] *Hella KGaA Hueck and Company. Lighting Technology*. [Online]. Available: http://www.hella.com/hella-com/assets/media_global/TI_Lichttechnik_en.pdf
[25] S. S. Welch, "Effects of window size and shape on accuracy of subpixel centroid estimation of target images," Nat. Atmos. Space Admin. Langley, Hampton, VA, NASA Tech. Paper 3331, Oct. 1993.
[26] A. Lopez, J. Hilgenstock, A. Busse, R. Baldrich, F. Lumbreras, and J. Serrat, "Nighttime vehicle detection for intelligent headlight control," in *Proc. 10th Int. Conf. Adv. Concepts Intell. Vis. Syst.*, 2008, vol. 5259, pp. 113–124.
[27] *CMOS Image Sensors of Aptina Imaging (n.d.)*. [Online]. Available: http://www.aptina.com/products/image_sensors/
[28] Y. Li, N. Haas, and S. Pankanti, "Intelligent headlight control using learning-based approaches," in *Proc. IEEE Intell. Veh. Symp.*, 2011, pp. 722–727.
[29] H. G. Jung, Y. H. Lee, H. J. Kang, and J. Kim, "Sensor fusion-based lane detection for LKS+ACC system," *Int. J. Autom. Eng.*, vol. 10, no. 2, pp. 219–228, Apr. 2009.
[30] P. E. Debevec and J. Malik, "Recovering high dynamic range radiance maps from photographs," in *Proc. Int. Conf. Comput. Graph. Interactive Tech.*, 1997, pp. 369–378.
[31] D. A. Forsyth and J. Ponce, "Radiometry—measuring light," in *Computer Vision, A Modern Approach*. Englewood Cliffs, NJ: Prentice-Hall, 2003, ch. 4, pp. 55–69.

Potential Accuracy of Traffic Signs' Positions Extracted From Google Street View

Wai Yeung Yan, *Member, IEEE*,
Ahmed Shaker, *Member, IEEE*, and Said Easa

***Abstract*—This work demonstrates the potential use of Google Street View (GSV) in engineering measurements. An investigation was conducted to assess the geopositioning accuracy of traffic signs extracted from GSV. A direct linear transformation (DLT) model is used to establish the relationship between the GSV image coordinate system and the ground coordinate system with the aid of ground control points (GCPs). The ground coordinates of the traffic sign can be retrieved by using the solved DLT coefficients. It is found that the root-mean-square (RMS) error of the extracted traffic sign's location is less than 1 m in general. By increasing the number of GSV images and GCPs, the RMS error can be further reduced to 0.5 m or less. This preliminary study demonstrates a viable solution to extract the location of traffic signs from GSV.**

***Index Terms*—Direct linear transformation (DLT), Google Street View (GSV), ground control points (GCPs), traffic sign.**

I. Introduction

Database construction of roads and highways is one of the big challenges that involve a balance between the data acquisition cost and the required level of details. Identification and extraction of road features play a key role in the development of road inventory system and maintenance. Previously, extraction of 2-D and 3-D road alignments [1], [2], moving vehicles [3], road markings [4], and streetlight poles [5] was conducted using aerial photogrammetry and satellite remote sensing techniques. Although the effectiveness of these techniques in extracting the road features has been demonstrated, limited spatial resolution, relief displacement, and shadowing effect resulted in a challenge to identify small traffic control devices, such as traffic signs. A mobile mapping system (MMS) can mostly resolve the problem with ground-based data captured at a high level of detail. The MMS requires the use of high-end equipment such as panoramic cameras, laser scanners, Global Positioning System (GPS), and inertial navigation system (INS) sensors [6]. The operational cost is directly impacted by the scale required for data acquisition. Recently, free-to-the-public geospatial data have been offered by public and private agencies. Examples include Google Earth, Microsoft Bing Map, Nokia 3-D, OpenStreetMap, USGS EarthExplorer, and Yahoo Maps. Users are encouraged to access such free data and services to support their operations; this thus inspires the authors to evaluate the use of Google Street View (GSV) as an example to one of these existing free geospatial data, to extract accurate geographic locations of traffic signs for the construction of road inventory.

GSV, which was first launched in 2007, provides panoramic views at the street level for cities in more than 20 countries. GSV is captured by an MMS including laser scanners, high-speed video cameras, high-resolution cameras, GPS, wheel encoder, INS, and a rack of computers that can be mounted on different vehicular platforms [7]. With the huge amount of collected data, a set of algorithms was developed for sensor fusion, map matching, panoramic stitching, facade texture mapping, and 3-D modeling. Intensive effort has been made for privacy protection such as detecting and blurring human faces and license plates [8]. After postprocessing, the panoramic imagery with varying zoom levels was generated and stored in distributed servers around the world.

In this paper, instantaneous screen capture of GSV images was used to determine the location of a traffic road sign. In spite of the numerous literatures regarding automatic traffic sign detection and recognition, this study focuses on modeling the image orientation of GSV, which is a key step to retrieve accurate geographic coordinates of the detected traffic signs.

II. Methodology

The ultimate goal of this work aims to automatically extract traffic sign locations using the overall workflow as shown in Fig. 1. GSV can be displayed in an Internet browser with Flash plug-in through the Google Maps API object *GstreetviewPanorama*. The GSV instantaneous screen image can be captured from the browser, and the image coordinate system is denoted by (u, v). Traffic sign post can be detected in the GSV image by using template-matching and decision fusion techniques from which the location of the traffic sign (u_t, v_t) in the GSV local image coordinate system can be retrieved. However, the focus of this short paper is to determine the geographic location of the traffic sign in the ground coordinate system (X, Y, Z) to construct and update the road and highway databases. The relationship between the image and the ground coordinate systems can be established using the well-known close-range photogrammetry model, i.e., direct linear transformation (DLT). The model requires a number of control points identified on the image and the ground in their corresponding coordinate system so as to determine the DLT coefficients. The ground (object) coordinates (X_t, Y_t, Z_t) of any traffic sign location can be determined by using the solved DLT coefficients and the traffic sign

Manuscript received February 16, 2012; revised July 6, 2012 and October 3, 2012; accepted December 6, 2012. Date of publication January 9, 2013; date of current version May 29, 2013. This work was supported in part by the Natural Sciences and Engineering Research Council of Canada under a Discovery Grant. The Associate Editor for this paper was N. Papanikolopoulos.

The authors are with the Department of Civil Engineering, Ryerson University, Toronto, ON M5B 2K3, Canada (e-mail: waiyeung.yan@ryerson.ca).

Color versions of one or more of the figures in this paper are available online at http://ieeexplore.ieee.org.
Digital Object Identifier 10.1109/TITS.2012.2234119